Delay time embedding of mass loss avalanches in a fusion plasma-oriented sandpile model

C. A. Bowie, R. O. Dendy, and M. J. Hole

Citation: Physics of Plasmas **23**, 100703 (2016); doi: 10.1063/1.4964667
View online: http://dx.doi.org/10.1063/1.4964667
View Table of Contents: http://scitation.aip.org/content/aip/journal/pop/23/10?ver=pdfcov
Published by the AIP Publishing

Delay time embedding of mass loss avalanches in a fusion plasma-oriented sandpile model

C. A. Bowie,[1,a)] R. O. Dendy,[2,3] and M. J. Hole[1]
[1]Research School of Physics and Engineering, Australian National University, Canberra ACT 0200, Australia
[2]CCFE, Culham Science Centre, Abingdon, Oxfordshire OX14 3DB, United Kingdom
[3]Centre for Fusion, Space and Astrophysics, Warwick University, Coventry CV4 7AL, United Kingdom

(Received 18 June 2016; accepted 27 September 2016; published online 10 October 2016)

The sandpile paradigm is widely used to model aspects of the phenomenology of magnetically confined fusion (MCF) plasmas, including enhanced confinement, edge pedestals and, potentially, the impulsive energy and particle release process known as ELMing. Here we identify new points of contact between ELMing and the systemwide avalanches in a sandpile. We compare the quantified response [Calderon *et al.*, Phys. Plasmas **20**, 042306 (2014)] to increased fuelling of the time sequence of edge localised mode events in a series of similar Joint European Torus plasmas with the response to increased fuelling of the time sequence of systemwide avalanches in a sandpile model [Chapman *et al.*, Phys. Rev. Lett. **86**, 2814 (2001)] that has well established links to MCF plasma phenomenology. Both the probability density functions of inter-event time intervals, and delay time embeddings of event time sequences, at different fuelling rates, show common features and point to shared underlying physics. *Published by AIP Publishing.*
[http://dx.doi.org/10.1063/1.4964667]

Sandpile models[1,2] have been extensively used to simulate aspects of the global phenomenology of macroscopic plasma systems, in both magnetic confinement fusion[3–10] and space and astrophysics.[11–20] In the sandpile paradigm, the system is typically fuelled by the addition of grains at its centre. If, as a consequence of fuelling, the local gradient of the sandpile exceeds a specified critical value Z_c, then local redistribution of sand takes place, following a simple algorithm. The resulting local movement of sand may cause the local gradient to exceed the critical gradient at neighbouring points, triggering further redistribution of sand there. This may continue progressively, giving rise to an avalanche, which may halt before it leaves the system, or propagate to the system boundary. The latter case is a systemwide avalanche, a category which provides a focus for the present paper. After each avalanche, the local gradient is everywhere at a value below critical. In the classical sandpile paradigm (as distinct from the running variant,[18,19] discussed further below), only then does fuelling recommence. The distribution of avalanche events, with respect to magnitude and their sequence in time, assists statistical characterisation of the system dynamics. The key components of the sandpile paradigm are thus energy fuelling, storage, and release through nonlocal nondiffusive transport events conditioned by a critical gradient. These map across to key aspects of the observed phenomenology of macroscopic plasma systems, hence the continuing topicality of sandpiles in plasma physics research.

Carreras *et al.*[3] and Newman *et al.*[4] first proposed sandpile models to interpret non-diffusive transport events, together with the associated radial temperature and density profiles, in magnetically confined fusion (MCF) plasmas. They conjectured that these profiles might lie close to the critical values for the onset of instabilities, driven to this state by externally applied heating. In this near-marginal state, a locally excited fluctuation could propagate radially: the resulting enhanced local transport would suppress the fluctuation by flattening the local profile, but this would cause steepening of the profile at neighbouring locations. This in turn would trigger local instability, thus propagating an avalanche. Evidence supporting the sandpile approach is also obtained from direct observation of avalanche events in experiments and numerical simulations, particularly where event statistics are power law or strongly non-Gaussian. Such observations are widespread in space and laboratory plasma systems.[16,17,20] The sandpile paradigm is also attractive in that it enables global modelling to be carried out, albeit at a relatively coarse-grained level, for plasma systems that are too computationally expensive to simulate using the first-principles equations of plasma physics. This reflects the fact that macroscopic plasmas are complex systems, whose global phenomenology emerges from the interaction of multiple physical processes, coupled across a very broad range of lengthscales and timescales. The sandpile paradigm has assisted understanding, in fusion plasmas, of the existence of different classes[21] of energy confinement regimes.[7–10] In solar-terrestrial and astrophysical plasma physics, the sandpile paradigm has been used successfully to help interpret impulsive energy release events originating in the magnetosphere,[11,13,14] the solar corona,[15] and accretion discs.[12]

Edge localised modes (ELMs) are pulsed relaxation events that typically accompany enhanced confinement regimes in magnetically confined toroidal plasmas. Understanding the ELMing process is central to research into the physics of large tokamak experiments such as the Joint European Torus (JET), and to the success of future burning plasma experiments in ITER.[22–24] The ELMing process encompasses both the birth-to-death life cycle of each individual ELM, and the way in which the sequence of many

a)Electronic mail: craig.bowie@anu.edu.au

successive ELMs arises under specific plasma conditions. The characterisation of measured sequences of inter-ELM time intervals from the perspective of statistical physics and complex systems science was pioneered in Refs. 25 and 26. For JET plasmas in particular, this approach has recently produced results which are novel and unexpected. These include period doubling of type-I ELMing in a sequence of similar JET plasmas in response to different gas puffing rates;[27] first principles differentiation between type-I and type-III ELMs for a large sample of JET plasmas, in terms of extreme value distributions of inter-ELM time intervals;[28] and the identification of structure in the distribution of inter-ELM time intervals from a uniquely long and consistent sequence of 151 quasi-identical JET plasmas.[29] In the present paper, we build on a recent study by Calderon *et al.*[27] of the sequence of inter-ELM time intervals in a group of similar JET plasmas, which differ only in the rate at which they are fuelled through gas puffing at the outer plasma edge. This set of plasmas yields clear evidence[27] of low dimensional system dynamics in the ELMing process, including period doubling. Figure 1, reproduced from Calderon *et al.*, shows the probability distribution function (pdf) of inter-ELM intervals δt_n together with delay time embedding plots of δt_{n+1} versus δt_n for successive pairs of inter-ELM time intervals. The ELM occurrence times are defined, for present purposes, from the measured peaks of the recombination radiation signal D_α. The time interval $\delta t_n \equiv t_{n+1} - t_n$, where t_n is the measured occurrence time of the nth ELM, and t_{n+1} that of its immediate successor. Period doubling can be identified from the two peaks in the pdfs in Fig. 1, while the four discrete clusters of data points in the time delay plots reveal dynamical switching between the two periods. The question arises: what light does this newly identified phenomenology shed on the underlying physics of the ELMing process in these plasmas?

In the present paper, we address this question by identifying fresh parallels between ELMing and systemwide avalanches in a sandpile. The possibility that, in some circumstances, ELMing may resemble avalanching was raised[7] in studies of the specific sandpile model of Ref. 30. This simple one-dimensional N-cell sandpile model[7,30] incorporates other established models[2,31] as limiting cases. It is centrally fuelled at cell $n = 1$, and its distinctive feature is the rule for local redistribution of sand near a cell (say at $n = k$) at which the critical gradient Z_c is exceeded. The sandpile is conservatively flattened around the unstable cell over a fast redistribution lengthscale L_f, which spans the cells $n = k - (L_f - 1)$, $k - (L_f - 2), \ldots, k + 1$, so that the total amount of sand in the fluidization region before and after the flattening is unchanged. Because the value at cell $n = k + 1$ prior to the redistribution is lower than the value at the cells behind it, the redistribution results in the relocation of sand from the fluidization region, to the cell at $n = k + 1$. The system is then iterated to stability, resulting in an avalanche as redistribution is sequentially triggered outwards across neighbouring cells. An avalanche may, or may not, propagate right across the sandpile and result in mass loss from the edge, which we refer to as a mass loss event (MLE). The system

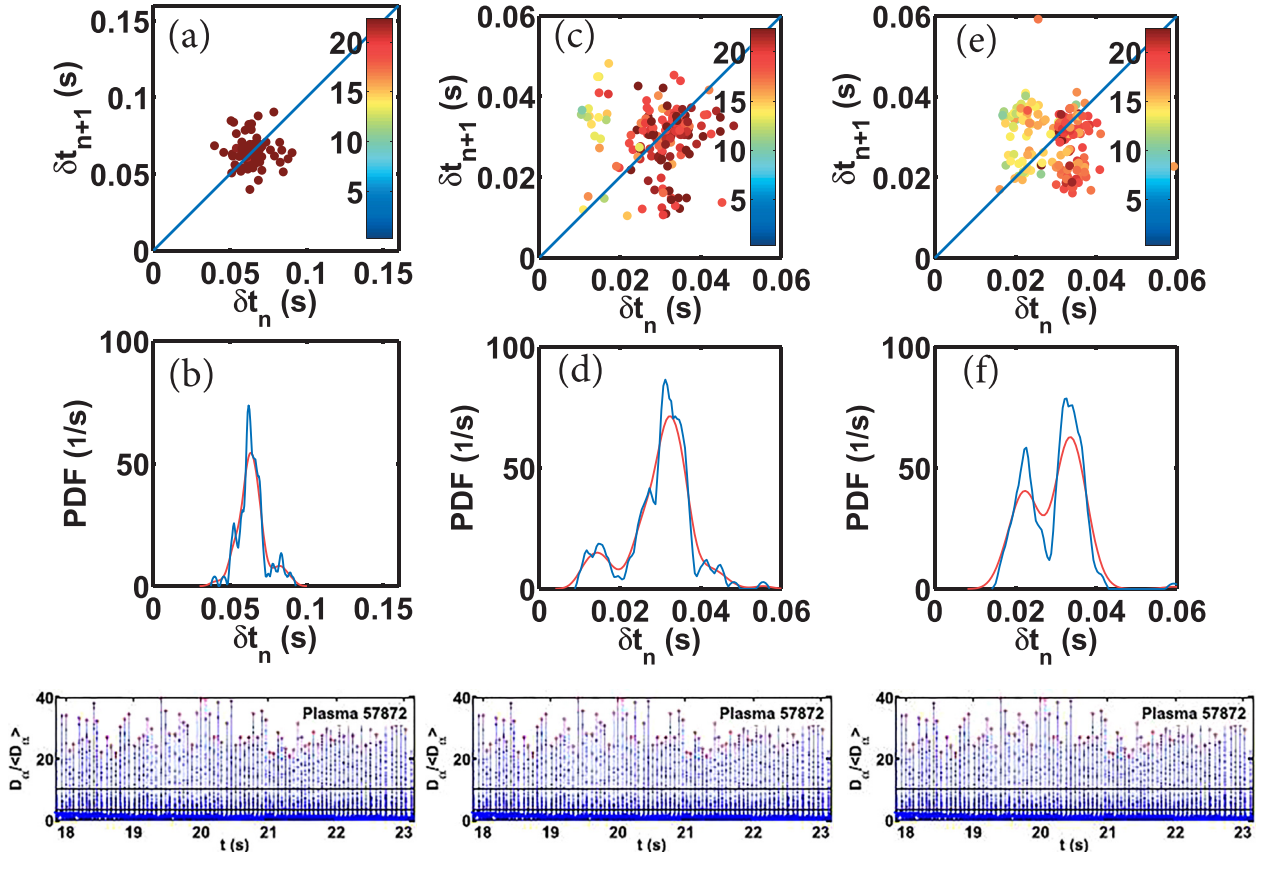

FIG. 1. pdfs, delay plots, and D_α plots for ELMs in JET plasmas, reproduced with permission from Calderon *et al.* Phys. Plasmas **20**, 042306 (2013). Copyright 2013 AIP Publishing. Gas puffing rate increases from left to right.

continues to be swept from left to right until no further grains of sand escape from the right hand edge. During these sweeps, the addition of sand is paused, and recommences only when sand ceases to escape, which we define as the end of the MLE. Intra-sandpile avalanches are ignored for the purposes of determining when an MLE has started and ended. If a systemwide avalanche is triggered by the addition of a given grain of sand at the centre, the magnitude of the associated MLE is defined to equal the total amount of sand lost once the sandpile has iterated to stability, prior to addition of the next grain. The lengthscale L_f, normalized to the system scale N, provides the model's primary control parameter L_f/N, which governs different regimes of avalanche statistics and system dynamics. A further control parameter is the ratio between Z_c and the amount of sand, dx, added at each time step. Unlike some previous implementations of the model,[6–8,10,32] Z_c here is single valued, rather than fluctuating randomly within a narrow range. The phenomenology generated by this model is known to include several features resembling tokamak plasmas, including edge pedestals, enhanced confinement,[7] and self-generated internal transport barriers.[10] Potentially related to ELMs—we explore this conjecture in this paper—are the systemwide avalanches resulting in MLEs. The character of the MLE sequences varies with the confinement properties of the sandpile, exhibiting interesting quantitative correlations. For example, the mean time interval between MLEs scales with the energy stored in the sandpile, in a way, resembles the scaling of the mean time intervals between ELMs and the stored energy in some JET plasmas.[7] We emphasise that the mass loss events, whose time series we analyse in relation to ELM time series, correspond to systemwide avalanches only. Their time series

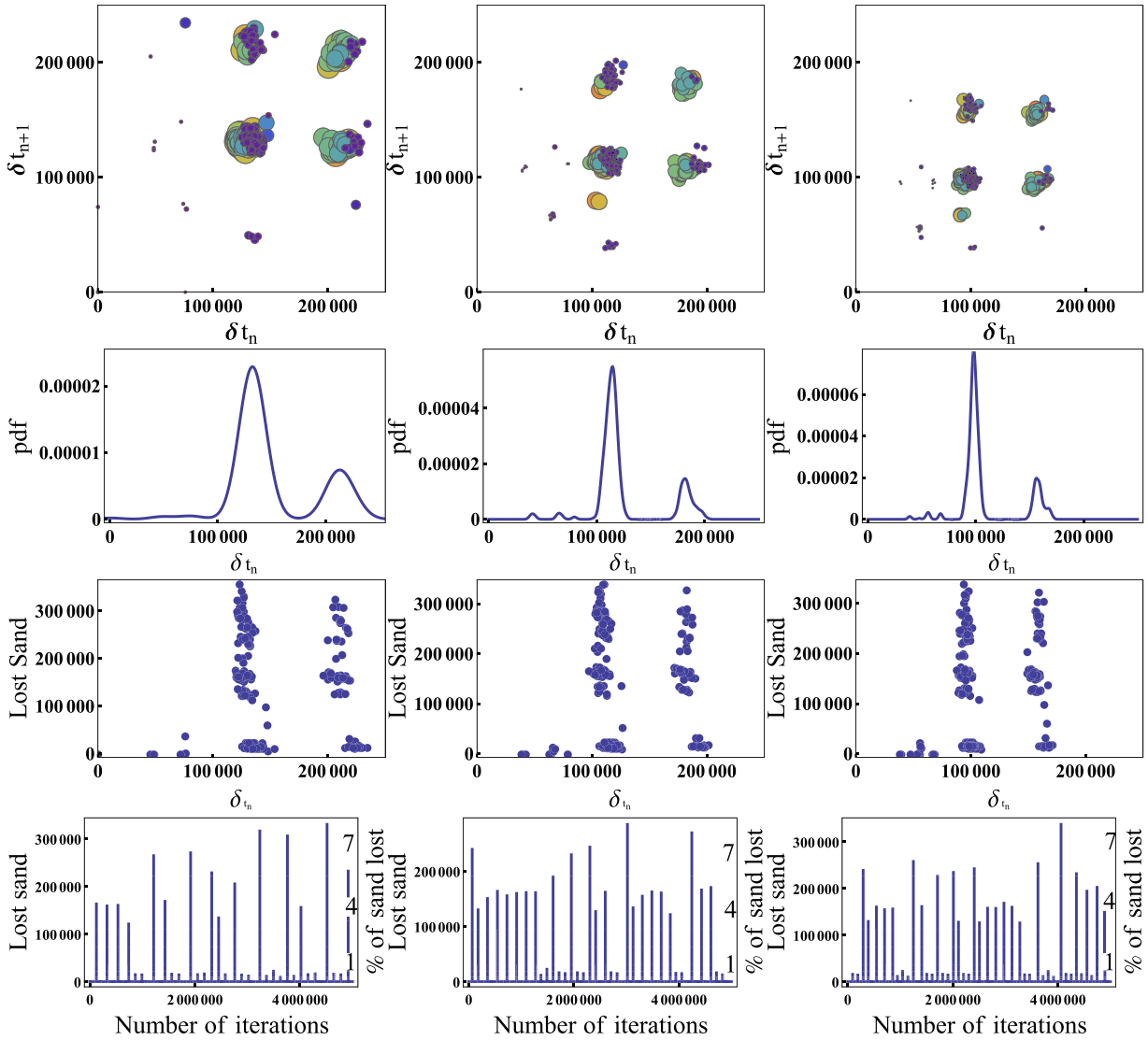

FIG. 2. Delay plots (top), pdfs (second row), MLE size (third row), and lost sand plots (bottom) for dx (dx/Z_c) = (left) 0.72 (0.006), (centre) 0.84 (0.007), and (right) 0.96 (0.008) (original model). In each case, $Z_c = 120$, $L_f = 5$, and results are shown for 50×10^6 iterations (5×10^6 iterations for the lost sand plots) in steady state, i.e., after the sandpile has filled. Horizontal and vertical axes represent: δt_n, δt_{n+1} (delay plots); δt_n, proportion of occurrences (pdfs); δt_n, amount of sand lost (MLE size); and time, amount of sand lost per iteration (lost sand plots). In the lost sand plots, an additional right hand axis shows the percentage of total sand lost during the avalanche, compared with the average amount of sand in the sandpile in steady state. Lost sand plots show the amount of sand lost during each avalanche, rather than each iteration. Fuelling is paused during avalanches until the sandpile ceases avalanching. Bubble size and colour represent MLE size in delay plots (small (blue) to large (red)). The smallest bubbles represent MLEs of about 600 units, while the largest bubbles represent MLEs of about 3×10^5 units.

and overall statistics are therefore constrained by the system size together with the fuelling rate and critical gradient. In consequence, one does not expect scale-free self-organised criticality (SOC)-type statistical properties for these events. For the sandpile model that we use, it is known from Ref. 30 that the distribution of internal avalanches (which do not result directly in external mass loss, and hence are not regarded in this paper as proxy ELMs) can indeed exhibit scale-free SOC-type characteristics. As noted in Ref. 33, SOC may be present regardless of whether or not exponential waiting times are observed, so that in the present case the absence of scale-free behaviour in relation to both MLE size and waiting times is not an indicator of the presence or absence of SOC.

Prompted by the recent discovery[27] (see Fig. 1) of low dimensional behaviour in the dependence of the sequence of inter-ELM time intervals on the particle fuelling rate from gas puffing in some JET plasmas, we investigate here whether the sequence of inter-MLE time intervals from the sandpile of Refs.7 and 30 depends analogously on the sandpile fuelling rate. We simulate centrally fuelled sandpiles for different values of Z_c, L_f, and dx, and the system is iterated until stable probability distribution functions of waiting times emerge. The fraction of sand lost in a large MLE is typically 5% of the total, which is comparable with the fraction of total plasma magnetic energy lost in a large ELM.

Figures 2 and 3 show examples of results produced by the model, dependant upon the fuelling rate, dx. To assist comparison with the ELM results of Figure 1, Figures 2 and 3 show a selection of pdfs of waiting times, δt_n, from the start of an MLE to the start of the following MLE, and delay plots of δt_n against δt_{n+1}, as well as the time series of MLEs.

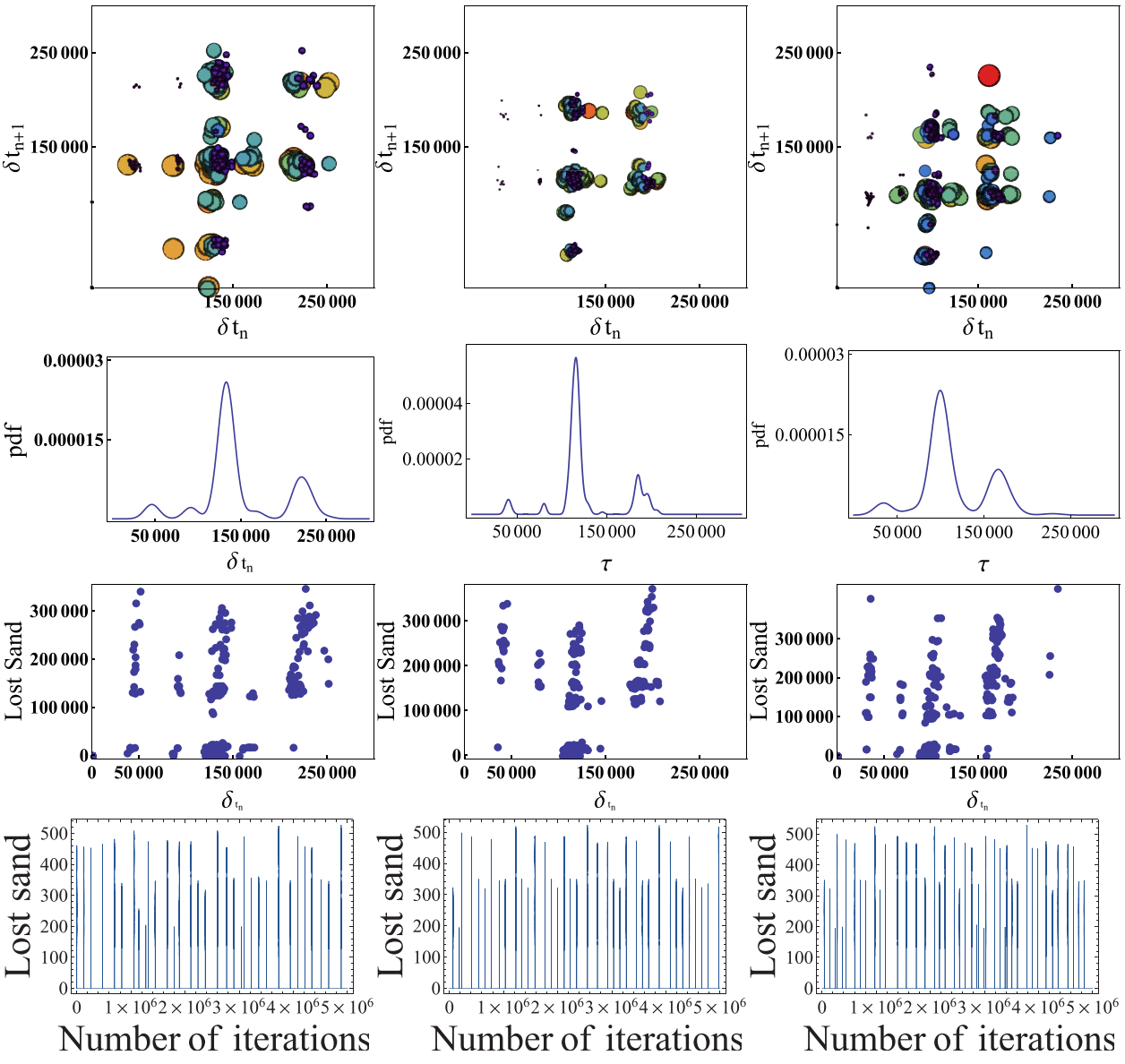

FIG. 3. Delay plots (top), pdfs (2nd row), MLE size (3rd row), and lost sand plots (bottom) for dx $(dx/Z_c) =$ (left) 0.72 (0.006), (centre) 0.84 (0.007), and (right) 0.96 (0.008) (running model). In each case, $Z_c = 120$, $L_f = 5$, and the results are shown for 50×10^6 iterations (5×10^6 iterations for the lost sand plots) in steady state, i.e., after the sandpile has initially filled. Horizontal and vertical axes represent: $\delta t_n, \delta t_{n+1}$ (top panels: delay plots); δt_n, proportion of occurrences (2nd row: pdfs); δt_n, MLE size (3rd row: MLE size); and time and amount of sand lost per iteration (bottom panels: lost sand plots). In the pdfs, $\delta t_n < 1000$ is not shown, in order to make the behaviour clearer at larger values of δt_n. In the top panels, bubble size and colour represent MLE size (small (blue) to large (red)). The smallest bubbles represent MLEs of about 600 units, while the largest bubbles represent MLEs of about 3×10^5 units.

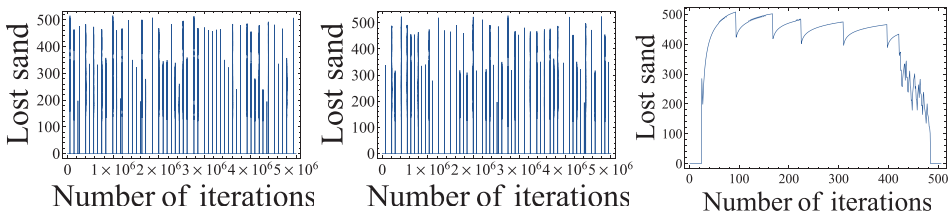

FIG. 4. Lost sand plots for the running sandpile model. Left and centre panels show lost sand plots for dx (dx/Z_c) = 1.08 (0.009) and 1.2 (0.01). The right panel shows an expanded view of the rightmost vertical stripe in the left sub-figure, which runs over approximately 400 iterations. At each iteration, dx units of sand are added, and a systemwide avalanche occurs. Following the first avalanche, the system becomes unstable, meaning that the avalanche would continue over many iterations, even if no further sand were added (as occurs in the classic model, in which addition of sand is suspended until avalanching ceases). The amount of sand lost at each iteration in the example shown is approximately 400–500 units. The overall profile of sand loss during the running sandpile MLE (right) comprises a series of smooth increases followed by drop-offs, before declining noisily after about 400 iterations, followed by complete cessation after about 480 iterations. This behaviour is typical for a large MLE. The full scale lost sand plots (left and centre) show that the amount of sand lost following a systemwide avalanche remains zero while the sandpile rebuilds through internal avalanches in response to continuing fuelling, until the next systemwide avalanche commences. The amount of sand lost in each systemwide avalanche varies from approximately 600 units to approximately 3×10^5 units. The waiting time between systemwide avalanches is shown in the delay time pdfs (see Figure 3).

The delay plots, pdfs, and time series of MLEs are for common values of Z_c and L_f, and are obtained for multiple values of the fuelling rate dx in the low fuelling regime $dx/Z_c \leqslant 0.01$.

Figure 2 shows the results from the sandpile model of Refs. 4 and 30, while Figure 3 shows results from a new running version of this model, which we now introduce. Our objective here is to test the robustness of the quantitative MLE phenomenology against minor variations of the sandpile model adopted. Whereas in models which follow[4,30] the approach of Ref. 1, the sandpile is iterated to stability after addition of the nth grain before the $(n+1)th$ grain is added; this is not the case in the running sandpile[18,19] approach. Instead sand grains are added at intervals, regardless of whether the system has iterated to stability. Specifically, a grain is added after each sweep of the sandpile redistribution algorithm from the centre to the edge. This defines a *de facto* timestep. It follows that sand can be added while a systemwide avalanche is under way, hence "running." A systemwide avalanche from our running sandpile is defined to continue for as long as sand is lost from the final cell at each successive time step. Systemwide avalanches in the running sandpile model thus have a time dependent profile of lost sand, whereas in the original model systemwide avalanches are impulsive in time. The magnitude of an MLE in the running version is determined by summing the sand lost between the first and last timestep of a systemwide avalanche. With this definition, we find that the MLE sizes for the original and running models are broadly similar.

For the running sandpile model, lost sand plots can resolve the amount of sand lost at each iteration, as well as the total amount of sand lost in an MLE, which typically continues for approximately 500 time steps. In order to see the time resolved behaviour of an MLE, an expanded view of a single vertical stripe in the lost sand plot is shown in the right hand panel of Figure 4. As noted in Ref. 33, different methods may be employed for measuring the time between MLEs; in the present case, we use the time from the start of one MLE to the start of the next. As the average MLE takes approximately 400–500 time steps, and the average waiting time is of the order of 100 000 time steps, there is little difference between this method and the "quiet time" method also discussed in Ref. 33.

For the cases shown in Figure 3, two peaks appear, defining two characteristic time intervals between MLEs. Each combination of the two characteristic waiting times appears in the delay plots. Similar behaviour is observed in Figure 1(c), where two characteristic waiting times are present, and four groupings of points appear in the delay plot. These groupings correspond to representing the four possible combinations of short waiting times following short, long following long, and long following short and *vice versa*. The MLE size plots in Figures 2 and 3 show that the MLE size is not correlated with the waiting time; both large and small MLEs occur for both short and long waiting times. The presence of such dynamical switching in each of Figures 1–3 suggests that an underlying dynamical principle may be responsible for the observed response to increased fuelling in both ELMing and sandpile cases.

The sandpile models used here are deterministic, with all variables kept constant during each run. The sequences of mass loss events (MLEs) have interesting points of similarity with those of the ELMs studied in Ref. 27. This suggests that ELMing phenomenology may include features that can be considered in terms of systemwide avalanching in the edge plasma, conditioned by the fuelling rate in relation to a critical gradient determined by the underlying plasma physics.

The similarities identified here in the differential response to increased fuelling rates in the time series of JET ELMs and of sandpile MLEs suggest that each ELM incorporates avalanche-type physics. Specifically, the avalanches to which this analogy applies are systemwide. These constitute the emptying of all the free energy stored in the sandpile, triggered by the addition of a "final grain," as distinct from the far more frequent internal avalanches, which occur as the sandpile rises, without losing mass or energy to its boundary. A full nonlinear kinetic-transport-magnetohydrodynamic model for the birth-to-death ELMing cycle has not yet been constructed. The present study reinforces the physical basis for anticipating that critical gradient-conditioned physics, combined with a relatively minor trigger, will lead to full plasma pedestal emptying. It also supports the suggestion that intra-ELM pedestal building in MCF plasmas may incorporate discontinuous transport processes having some of the character of internal avalanches.

The authors thank S. C. Chapman for helpful conversations. This work was jointly funded by the Australian

Research Council through Grant No. FT0991899 and the Australian National University. This work was part-funded by the RCUK Energy Programme [under Grant No. EP/I501045] and the European Communities. The views and opinions expressed herein do not necessarily reflect those of the European Commission. One of the authors, C. A. Bowie, is supported through an ANU Ph.D. scholarship and an Australian Institute of Nuclear Science and Engineering Postgraduate Research Award.

[1]P. Bak, C. Tang, and K. Wiesenfeld, Phys. Rev. A **38**, 364 (1988).
[2]R. O. Dendy and P. Helander, Phys. Rev. E **57**, 3641 (1998).
[3]B. A. Carreras, D. Newman, V. E. Lynch, and P. H. Diamond, Phys. Plasmas **3**, 2903 (1996).
[4]D. E. Newman, B. A. Carreras, P. H. Diamond, and T. S. Hahm, Phys. Plasmas **3**, 1858 (1996).
[5]R. O. Dendy and P. Helander, Plasma Phys. Controlled Fusion **39**, 1947 (1997).
[6]S. C. Chapman, R. O. Dendy, and G. Rowlands, Phys. Plasmas **6**, 4169 (1999).
[7]S. C. Chapman, R. O. Dendy, and B. Hnat, Phys. Rev. Lett. **86**, 2814 (2001).
[8]S. C. Chapman, R. O. Dendy, and B. Hnat, Phys. Plasmas **8**, 1969 (2001).
[9]J. P. Graves, R. O. Dendy, K. I. Hopcraft, and E. Jakeman, Phys. Plasmas **9**, 1596 (2002).
[10]S. C. Chapman, R. O. Dendy, and B. Hnat, Plasma Phys. Controlled Fusion **45**, 301 (2003).
[11]S. C. Chapman, N. W. Watkins, R. O. Dendy, P. Helander, and G. Rowlands, Geophys. Res. Lett. **25**, 2397, doi:10.1029/98GL51700 (1998).
[12]R. O. Dendy, P. Helander, and M. Tagger, Astron. Astrophys. **337**, 962 (1998); available at http://aa.springer.de/papers/8337003/2300962.pdf.
[13]N. W. Watkins, S. C. Chapman, R. O. Dendy, and G. Rowlands, Geophys. Res. Lett. **26**, 2617, doi:10.1029/1999GL900586 (1999).
[14]N. W. Watkins, M. P. Freeman, S. C. Chapman, and R. O. Dendy, J. Atmos. Sol.-Terr. Phys. **63**, 1435 (2001).
[15]D. Hughes, M. Paczuski, R. O. Dendy, P. Helander, and K. G. McClements, Phys. Rev. Lett. **90**, 131101 (2003).
[16]R. O. Dendy and S. C. Chapman, Plasma Phys. Controlled Fusion **48**, B313 (2006).
[17]R. O. Dendy, S. C. Chapman, and M. Paczuski, Plasma Phys. Controlled Fusion **49**, A95 (2007).
[18]T. Hwa and M. Kardar, Phys. Rev. A **45**, 7002 (1992).
[19]D. E. Newman, R. Sanchez, B. A. Carreras, and W. Ferenbaugh, Phys. Rev. Lett. **88**, 204304 (2002).
[20]R. Sanchez and D. Newman, Plasma Phys. Controlled Fusion **57**, 123002 (2015).
[21]F. Wagner, Plasma Phys. Controlled Fusion **49**, B1 (2007).
[22]H. Zohm, Plasma Phys. Controlled Fusion **38**, 105 (1996).
[23]A. Loarte, G. Saibene, R. Sartori, D. Campbell, M. Becoulet, L. Horton, T. Eich, A. Herrmann, G. Matthews, N. Asakura *et al.*, Plasma Phys. Controlled Fusion **45**, 1549 (2003).
[24]R. J. Hawryluk, D. J. Campbell, G. Janeschitz, P. R. Thomas, R. Albanese, R. Ambrosino, C. Bachmann, L. Baylor, M. Becoulet, I. Benfatto *et al.*, Nucl. Fusion **49**, 065012 (2009).
[25]A. W. Degeling, Y. R. Martin, P. E. Bak, J. B. Lister, and V. Llobet, Plasma Phys. Controlled Fusion **43**, 1671 (2001).
[26]J. Greenhough, S. C. Chapman, R. O. Dendy, and D. J. Ward, Plasma Phys. Controlled Fusion **45**, 747 (2003).
[27]F. A. Calderon, R. O. Dendy, S. C. Chapman, A. J. Webster, B. Alper, R. M. Nicol, and JET EFDA Contributors, Phys. Plasmas **20**, 042306 (2013).
[28]A. J. Webster and R. O. Dendy, Phys. Rev. Lett. **110**, 155004 (2013).
[29]A. J. Webster, R. O. Dendy, F. A. Calderon, S. C. Chapman, E. Delabie, R. Felton, T. N. Todd, F. Maviglia, J. Morris, V. Riccardo, B. Alper, S. Brezinsek, P. Coad, J. Likonen, M. Rubel, and JET EFDA Contributors, Plasma Phys. Controlled Fusion **56**, 075017 (2014).
[30]S. C. Chapman, Phys. Rev. E **62**, 1905 (2000).
[31]P. Bak, C. Tang, and K. Wiesenfeld, Phys. Rev. Lett. **59**, 381 (1987).
[32]S. C. Chapman, R. O. Dendy, and N. W. Watkins, Plasma Phys. Controlled Fusion **46**, B157 (2004).
[33]R. Sanchez, D. E. Newman, and B. A. Carreras, Phys. Rev. Lett. **88**, 068302 (2002).